J. Fluid Mech. (2020), *vol*. 905, A19. © The Author(s), 2020.
Published by Cambridge University Press
doi:10.1017/jfm.2020.752

Polymer-induced flow relaminarization and drag enhancement in spanwise-rotating plane Couette flow

Yabiao Zhu[1], Jiaxing Song[1], Nansheng Liu[1,†], Xiyun Lu[1] and Bamin Khomami[2,†]

[1]Department of Modern Mechanics, University of Science and Technology of China, Hefei Anhui 230026, PR China

[2]Department of Chemical and Biomolecular Engineering, University of Tennessee, Knoxville, TN 37996, USA

(Received 10 April 2020; revised 31 August 2020; accepted 5 September 2020)

Direct numerical simulation of polymer-induced flow relaminarization of turbulent spanwise-rotating plane Couette flow (RPCF) is reported for the first time. Specifically, the reverse transition pathway from a Newtonian turbulent RPCF to a fully relaminarized drag enhanced viscoelastic flow has been elucidated. Evidently, this transition occurs gradually by weakening and eventual elimination of small-scale vortices as the Weissenberg number (Wi) is enhanced, paving the way for a two-dimensional laminar flow consisting of large-scale and highly organized roll cells. The influence of polymer additives on convective momentum exchange by large-scale roll cells and small-scale turbulent vortices, namely, the drag reduction (DR) realized by elimination of turbulent vortices and the significant drag enhancement (DE) that results from polymer roll cell interactions has been identified as the mechanism of DE. The observed vortical changes point to a universal mechanism for the coupling of polymer chains and turbulent vortices in wall-bounded viscoelastic DE and DR flows.

Key words: viscoelasticity, rotating turbulence

1. Introduction

As a curvature-free limit of Taylor–Couette flow (TCF), the spanwise-rotating plane Couette flow (RPCF) has been known to share many dynamical properties with TCF (Tsukahara, Tillmark & Alfredsson 2010; Brauckmann, Salewski & Eckhardt 2016), namely, analogous transitions from laminar to turbulent flow at different combinations of the same key driving forces, i.e. shear rate gradient and the system rotation quantified as the shear Reynolds (Re) and rotation (Ro) numbers, respectively (Dubrulle *et al.* 2005; Grossmann, Lohse & Sun 2016). In fact, several similar turbulent flow regimes have been identified in the (Re, Ro) parameter space in RPCF and TCF (Andereck, Liu & Swinney 1986; Tsukahara *et al.* 2010). These flow regimes are essentially characterized by large-scale vortical structures (roll cells for RPCF that are reminiscent of Taylor vortices) overlaid by small-scale turbulent vortices (Bech & Andersson 1996, 1997;

† Email addresses for correspondence: lns@ustc.edu.cn, bkhomami@utk.edu

Gai *et al.* 2016; Xia *et al.* 2019). These large-scale vortical structures have a cross-stream size of approximately the gap width and are streamwise-oriented and spanwise-organized; these structures are also known to play an important role in transverse momentum transport and in turn in the drag/torque features of the flow (Bech & Andersson 1997; Martínez-Arias *et al.* 2014; Salewski & Eckhardt 2015; Brauckmann *et al.* 2016; Gai *et al.* 2016). For example, in the turbulent RPCF at $Re = 1300$, the roll cells are found to facilitate a substantial enhancement of transverse momentum transport as they become more well-defined and energetic; specifically, the maximum drag is realized at an anticyclonic spanwise rotation $Ro \approx 0.2$ (Brauckmann *et al.* 2016; Gai *et al.* 2016).

Of interest, the RPCF at $Re = 1300$ and $Ro = 0.2$ has been identified as a flow regime termed 'contained turbulence in roll cells (CNT)' (Tsukahara *et al.* 2010; Gai *et al.* 2016). It is characterized by turbulence that seems to be contained in the roll cells and not connected to turbulence in neighbouring roll cells. According to Tsukahara *et al.* (2010), two typical transition pathways have been indicated for the RPCF of anticyclonic rotation to access this intriguing flow regime. One is realized by increasing Ro at a fixed Re, for example 800. It undergoes in sequence the flow regimes labelled 'featureless turbulence', 'turbulence with roll cells (TRC)' and, finally, CNT. The other is realized by decreasing Re while fixing $\Omega = Re\,Ro$ as a constant, for example 20. If started from the TRC, it goes through the CNT to the laminar Couette flows with stable roll cells of wavy three-dimensional (3-D) structure (COU3D), to that of meandering 2-D structure (COU2Dm) and then to that of straight 2-D structure (COU2Dh/COU2D). The sub-regimes COU3D, COU2Dm and COU2Dh/COU2D are indicated to have strong, weak and absent interplays between the neighbouring roll cells, respectively.

For viscoelastic turbulent TCF of a dilute polymeric solution, significant curvature dependence of drag enhancement (DE) has been reported due to flow transitions driven by significant changes in large-scale Taylor vortices (TV) (Liu & Khomami 2013*b*; Song *et al.* 2019). Specifically, in the high curvature limit (evaluated as the inner-to-outer radius ratio of $\eta = 0.5$), and in presence of polymer additives the large-scale Newtonian TV break down into small-scale Görtler vortices (GV) near the walls. These small-scale GV lead to much higher incoherent transport and homogenization of the polymer stress component $\tau^p_{r\theta}$ which in turn acts as a dominant source term in the angular momentum transport. Consequently, a drastic DE of 171 % is realized. In contrast, at a low curvature ($\eta = 0.912$), the large-scale TV persist and become better organized and more energetic, resulting in much higher coherent angular momentum flux (equivalent to the Reynolds stress) across the gap; hence, a much lower DE $\sim$72 % is realized. Undoubtedly, the role of vortical structures on momentum transport in viscoelastic TCF is intimately coupled with the flow curvature. To fundamentally understand this coupling the following question must be addressed: what is the flow response (including drag and vortical structure dynamics) to polymer additives in turbulent RPCF (zero curvature analogue of TCF) where only large-scale roll cells are present? In fact, the primary motivation of the current work is to answer this question.

In recent years, intriguing flow features have also been reported in turbulent viscoelastic plane Couette flows (PCF). Specifically, much weaker roll cells are observed as compared to their Newtonian counterparts (Pereira *et al.* 2017*a*,*b*; Teng *et al.* 2018). Commensurate with this change, as the polymeric elastic forces (commonly quantified in terms of the Weissenberg number Wi) increase, much weaker transverse momentum transfer is realized. Consequently, drag reduction (DR) of up to $\sim$34 % is observed in viscoelastic PCF at O(1) Wi. This is in contrast to the DE observed in turbulent viscoelastic TCF (Liu & Khomami 2013*b*; Song *et al.* 2019). The extent of the aforementioned DR is commensurate with formation of weaker quasi-streamwise vortices (QSV) in the near-wall

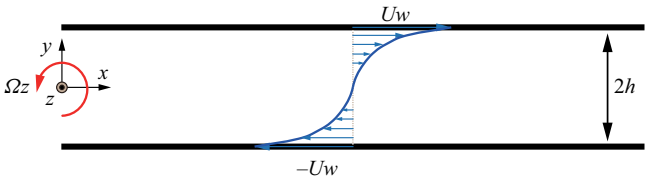

FIGURE 1. Sketch of spanwise-rotating plane Couette flow.

regions and elongated vortices away from the walls. This observation supports earlier findings that indicate polymer-induced DR has the same physical origin in wall-bounded flows, namely, the mean flow shear gradient renders significant polymer stretch in the near-wall region that acts to suppress the self-sustaining process of wall turbulence and in turn the Reynolds stress production (Sureshkumar, Beris & Handler 1997; Dubief *et al.* 2004; Li, Sureshkumar & Khomami 2006; Kim *et al.* 2007; White & Mungal 2008). Moreover, recent studies have shed light on the origin of the maximum drag reduction (MDR), namely, in this regime the flow dynamics is driven by an elasto-inertial instability (Dubief, Terrapon & Soria 2013; Samanta *et al.* 2013; Li, Sureshkumar & Khomami 2015; Sid, Terrapon & Dubief 2018) that could even eliminate Newtonian turbulence (NT). Furthermore, flow relaminarization has recently been observed in channel and pipe flows of polymeric solutions as polymer concentration (elasticity level) is increased at the transition Re (Choueiri, Lopez & Hof 2018; Lopez, Choueiri & Hof 2019; Shekar *et al.* 2019; Chandra, Shankar & Das 2020). Specifically, the MDR state is achieved via a reverse transition pathway from NT through a relaminarized state. These intriguing new observations bring up yet another interesting question: can elasticity-driven flow relaminarization occur in a turbulent RPCF where the flow dynamics is dominated by large-scale roll cells? Answering this question is the secondary goal of this study.

To answer the aforementioned two fundamentally questions, extensive high-fidelity direct numerical simulations (DNS) of viscoelastic RPCF (see figure 1) have been performed at $Re = 1300$, $Ro = 0.2$, $0 < Wi < 40$. To this end, we report for the first time polymer-induced flow relaminarization of turbulent RPCF which results in DE. The elastically driven fluid physics behind these major kinematics and frictional changes are also discussed.

2. Problem formulation and computational details

Similar to our earlier studies of polymer-induced DR in planar wall-bounded turbulent flows and elasto-inertial turbulence in TCF, DNS is performed via a fully spectral, three-dimensional parallel algorithm (Li *et al.* 2006, 2015; Liu & Khomami 2013*a*,*b*; Teng *et al.* 2018; Song *et al.* 2019). As indicated in figure 1, we have chosen h, h/U_w, U_w and $\rho U_w{}^2$ as scales for length, time, velocity $\boldsymbol{u}$ and pressure P, respectively. Here, $2h$ denotes the gap width, U_w is the wall translation velocity, ρ represents the solution density. The polymer stress $\boldsymbol{\tau}^p$ is related to the polymer conformation tensor $\boldsymbol{C}$ through the FENE-P (finitely extensible nonlinear elastic-Peterlin) constitutive model. The governing equations for an incompressible flow of FENE-P fluids are non-dimensionalized as

$$\nabla \cdot \boldsymbol{u} = 0, \tag{2.1}$$

$$\frac{\partial \boldsymbol{u}}{\partial t} + \boldsymbol{u} \cdot \nabla \boldsymbol{u} = -\nabla P + \frac{\beta}{Re}\nabla^2 \boldsymbol{u} + \frac{1-\beta}{Re}\nabla \cdot \boldsymbol{\tau}^p - Ro\boldsymbol{e}_z \times \boldsymbol{u}, \tag{2.2}$$

$$\frac{\partial \boldsymbol{C}}{\partial t} = -\boldsymbol{u}\cdot\nabla\boldsymbol{C} + \boldsymbol{C}\cdot\nabla\boldsymbol{u} + (\nabla\boldsymbol{u})^T\cdot\boldsymbol{C} - \boldsymbol{\tau}^p. \tag{2.3}$$

The polymer stress tensor $\boldsymbol{\tau}^p$ is obtained as

$$\boldsymbol{\tau}^p = \frac{1}{Wi}\left(\frac{L^2-3}{L^2-\mathrm{trace}(\boldsymbol{C})}\boldsymbol{C} - \boldsymbol{I}\right), \tag{2.4}$$

where $\beta = \eta_s/\eta_t$, with η_s and η_p being respectively the solvent and polymeric contributions to the total viscosity η_t, L signifies the maximum polymer chain extension and the Reynolds and rotation numbers are defined as $Re = \rho U_w h/\eta_t$ and $Ro = 2\Omega_z h/U_w$, respectively, with Ω_z being the spanwise system rotation. Weissenberg number is defined as $Wi = \lambda U_w/h$ where λ is the polymer relaxation time.

Following the numerical strategy for the spectral-based algorithm (Sureshkumar & Beris 1995; Sureshkumar *et al.* 1997), a small diffusive term $\kappa\nabla^2\boldsymbol{C}$ is added to (2.3) in the bulk flow region for numerical stabilization (Li *et al.* 2006, 2015; Teng *et al.* 2018; Song *et al.* 2019). Based on simulations performed at various Sc (see appendix), a κ value corresponding to a Schmidt number $Sc = 1/(\kappa Re) = 0.15$ has been used for all calculations. It is verified that such a Sc value does not modify the essential features of the velocity and polymer conformation fields. This Sc is of the same order as the value of 0.5 used to capture the elasticity-driven reverse transition occurring in pipe flows from the NT to elasto-inertial turbulence (EIT) regime via a flow relaminarization (Lopez *et al.* 2019), and close to $Sc = 0.2$ used to obtain the EIT developed in the PCF (Pereira *et al.* 2017*a*,*b*; Pereira, Thompson & Mompean 2019). Note that the original constitutive equation without the diffusive term is applied at the walls; thus no boundary conditions are imposed for $\boldsymbol{C}$ at solid boundaries.

All the simulations for viscoelastic RPCF are started from a statistically steady Newtonian turbulent state at $Re = 1300$ and $Ro = 0.2$ (Tsukahara *et al.* 2010; Gai *et al.* 2016). Large values of $\beta = 0.9$ and $L = 120$ are used to ensure the dilute polymeric solution has a nearly shear-independent viscosity and a significant elongational viscosity (scales with L^2). A comprehensive examination of elasticity-driven flow transition is performed by considering a broad range of $Wi = 0 \sim 40$. The computational domain is set as $L_x \times L_y \times L_z = 10\pi \times 2 \times 4\pi$ (Bech & Andersson 1996, 1997; Gai *et al.* 2016; Xia *et al.* 2019) for the streamwise, wall-normal and spanwise directions, respectively. According to the grid independence check (see appendix), we use a grid size of $N_x \times N_y \times N_z = 256 \times 129 \times 256$, which is much larger than those used for the Newtonian RPCF (Gai *et al.* 2016; Xia *et al.* 2019) but is required for accurate viscoelastic simulations. Following our prior study (Teng *et al.* 2018), a small time step, namely, $\Delta t = 0.01$ is used to ensure accuracy; calculations of $\sim 1000h/U_w$ are performed to ensure that a statistically steady flow state has been realized.

3. Results and discussion

The elasticity-driven flow relaminarization pathway is depicted in figure 2 through visualization of instantaneous vortical structures of the viscoelastic RPCF. Specifically, in the Newtonian flow (see figure 2*a*), large-scale roll cells are identified in the flow domain; they are essentially 3-D structures superimposed by small-scale turbulent vortices (QSV) in the near-wall region. According to Tsukahara *et al.* (2010), this flow corresponds to the flow regime labelled CNT. Evidently, once the polymer additive is introduced, the small-scale QSV near the walls are suppressed, giving rise to a great reduction in their number and intensity (see figure 2*b*). With the increase of Wi, further suppression of

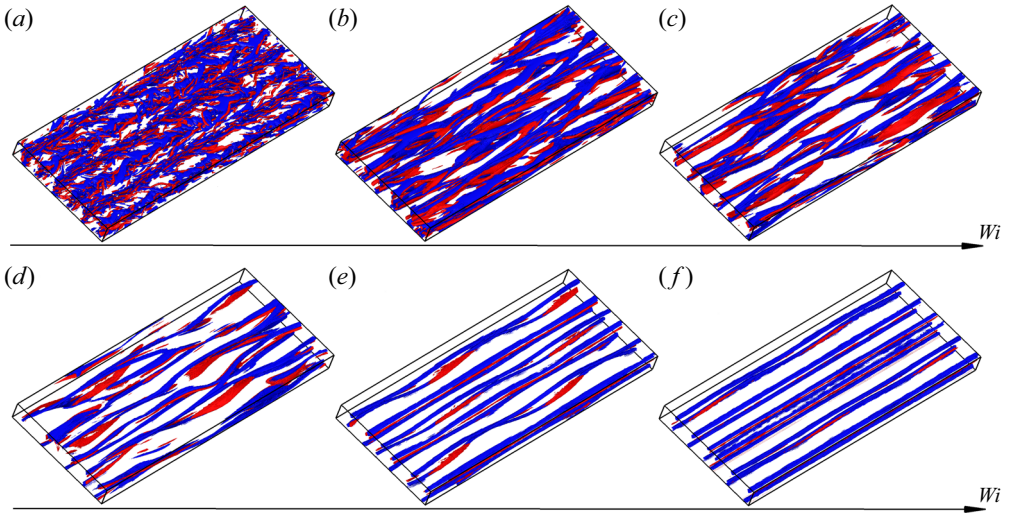

FIGURE 2. Flow relaminarization pathway visualized by instantaneous vortical structures that are identified by Q-criterion and coloured by the Q value (red/blue for positive/negative values). Q is defined as the difference between the magnitudes of fluid rotation and strain. (*a*) Newtonian, $Q = \pm 0.5$, $Re_\tau = 106.2$; (*b*) $Wi = 5$, $Q = \pm 0.1$, $Re_\tau = 114.9$, $DE = 17\,\%$; (*c*) $Wi = 10$, $Q = \pm 0.1$, $Re_\tau = 117.9$, $DE = 23\,\%$; (*d*) $Wi = 20$, $Q = \pm 0.1$, $Re_\tau = 120$, $DE = 28\,\%$; (*e*) $Wi = 30$, $Q = \pm 0.1$, $Re_\tau = 127.8$, $DE = 45\,\%$; (*f*) $Wi = 40$, $Q = \pm 0.1$, $Re_\tau = 130.5$, $DE = 51\,\%$.

small-scale turbulent vortices is observed, while the roll cells become more regular and meander in the streamwise direction (see figure 2*c–e*). Finally, at $Wi = 40$ (see figure 2*f*), the QSV usually referred to as turbulent vortices are totally eliminated and the roll cells occupy the entire flow domain. The roll cells have a 2-D structure, i.e. they have little to no variation in the streamwise direction. It corresponds to the flow sub-regime termed 'laminar Couette flow with straight 2-D roll cells', i.e. COU2Dh/COU2D (Tsukahara *et al.* 2010). This evinces that the viscoelastic RPCF has been relaminarized. A similar polymer-induced destruction of QSV or turbulent vortices has also been documented in the viscoelastic PCF where substantial DR is realized (Teng *et al.* 2018). However, great DE is obtained in the viscoelastic RPCF (see figure 2*a–f*). Here, DE factor is evaluated as $(Re_\tau^2 - Re_{\tau 0}^2)/Re_{\tau 0}^2$, where Re_τ and $Re_{\tau 0}$ are the frictional Reynolds numbers of the viscoelastic and Newtonian flows, respectively. The DE features and the fluid physics related to roll cell dynamics are discussed in detail below.

Polymer-induced changes leading to flow relaminarization can be quantified via the one-dimensional spectra (E_{uu}) of the streamwise turbulent kinetic energy (TKE) (see figure 3*a*). The most distinct variation in E_{uu} is observed at high wavenumbers. Specifically, a continuous decrease of several orders of magnitude over a broad range of wavenumbers occurs as Wi is increased. This observation is consistent with the enhanced suppression of turbulent vortices shown in figure 2 as well as a great reduction in contribution of small-scale fluctuating motions to TKE. As the viscoelastic RPCF becomes fully relaminarized at $Wi = 40$, E_{uu} shows a remarkable increase in its spectral peak value at wavenumber $k_z = 3$. This points to the fact that the roll cells have become more energetic and have a spanwise wavelength of approximately $L_z/3$ (see figures 2 and 4). As shown below, these large-scale roll cells greatly influence the transverse momentum transport across the gap.

Flow relaminarization is further evinced by the polymer-induced changes of unsteady characteristics of turbulent RPCF, illustrated in terms of the time series of near-wall

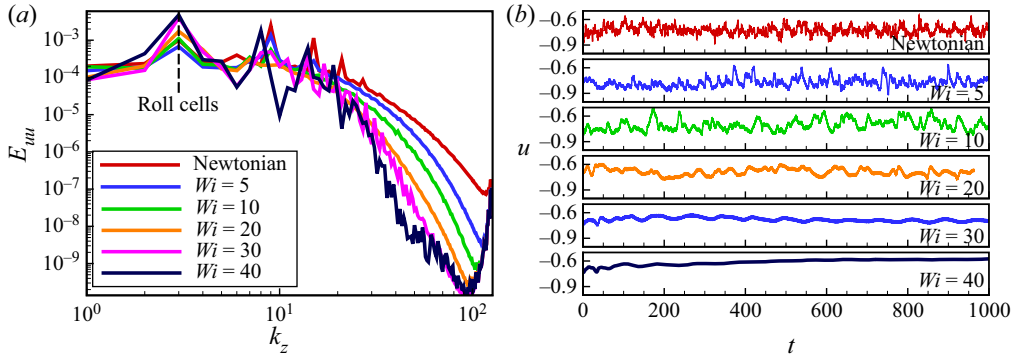

FIGURE 3. One-dimensional spectra of (*a*) the streamwise turbulent kinetic energy ($\langle u'u' \rangle$) at the channel centre and (*b*) time series of the near-wall streamwise velocity u sampled at $y = 0.97h$. Here, the fluctuating part of u is obtained as $u' = u - \langle u \rangle$; $\langle\,\rangle$ denotes hereafter the ensemble averaging.

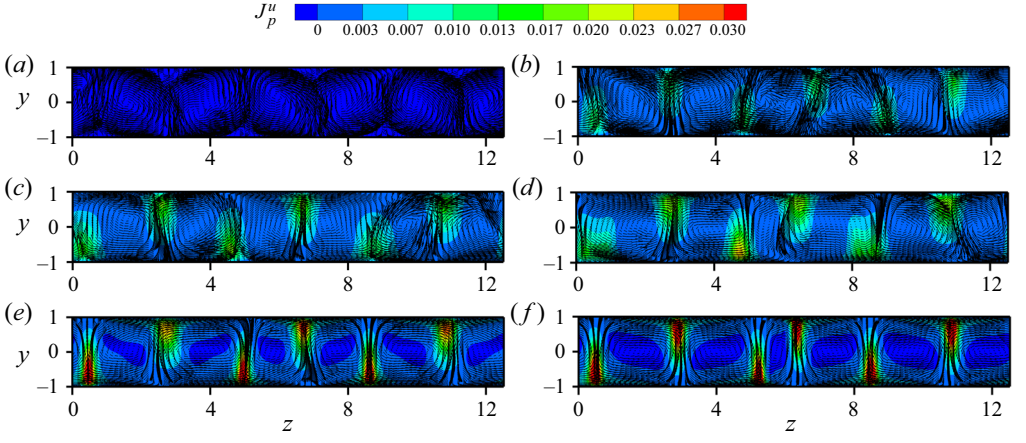

FIGURE 4. Instantaneous vortical structures visualized by streamline plots of the velocity vector (v, w) in the (y, z) plane at $x = L_x/2$ for (*a*) Newtonian flow, (*b*) $Wi = 5$, (*c*) $Wi = 10$, (*d*) $Wi = 20$, (*e*) $Wi = 30$ and (*f*) $Wi = 40$. The contour patterns are plotted based on the value of polymer stress term J_p^u.

streamwise velocity u (see figure 3*b*). For the Newtonian case, u is highly random in time, namely, high frequency fluctuations and significant intermittency are observed in the time series. Increasing Wi leads to a notable decrease of the fluctuating part of u especially at high frequencies as $Wi \geq 20$. When the viscoelastic turbulent RPCF transitions to a laminar flow at $Wi = 40$, u becomes steady, i.e. no temporal fluctuations are seen after a transition period, i.e. $t \sim 800h/U_w$. Moreover, as flow goes through a transition to a laminar flow state, the pairing of the large-scale counter-rotating roll cells arranged in the spanwise direction is not altered, i.e. it remains at three (see figure 4). Similar findings have been reported in our recent study of viscoelastic PCF when DR is observed (Teng *et al.* 2018). Hence, the answer to the second question posed in the introduction is a resounding yes.

The elasticity-driven transition to a laminar flow is accompanied with a monotonic increase in DE, i.e. up to 51 % at $Wi = 40$ (see figure 2). This is in stark contrast to viscoelastic channel and pipe flows where flow relaminarization gives rise to drastic DR

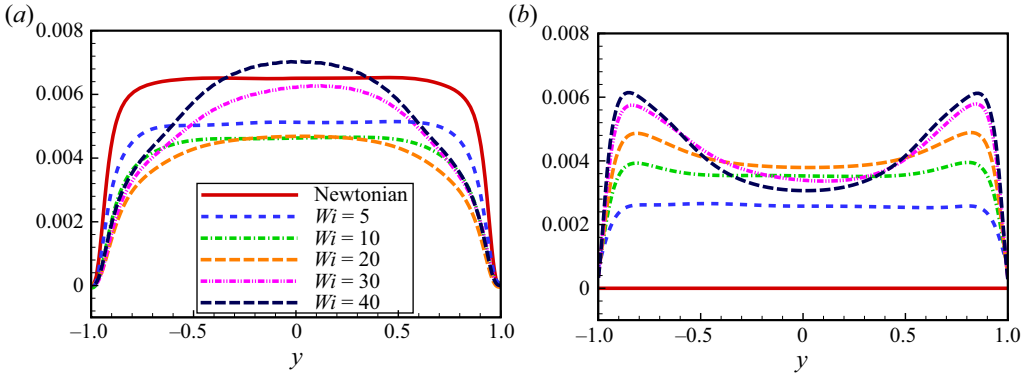

FIGURE 5. (*a*) Reynolds stress term J_R^u and (*b*) polymer stress term J_p^u.

(Choueiri *et al.* 2018; Lopez *et al.* 2019; Shekar *et al.* 2019; Chandra *et al.* 2020). To this end, the mechanism of DE is ascribed to momentum exchange modified by roll cells in the presence of polymers that evidently influence the force experienced at the channel walls and even between fluid layers across the gap (Teng *et al.* 2018). This force can be quantified in the context of the conserved momentum flux (Salewski & Eckhardt 2015; Brauckmann *et al.* 2016) as follows,

$$J^u = -\langle u'v' \rangle + \frac{\beta}{Re}\frac{\mathrm{d}\langle u \rangle}{\mathrm{d}y} + \frac{1-\beta}{Re}\langle \tau_{xy}^p \rangle. \tag{3.1}$$

The terms on the right-hand side of (3.1) in sequence are, the momentum flux associated with the Reynolds stress (J_R^u; convective flux), the viscous stress (J_v^u; diffusive flux) and the polymer stress (J_p^u; polymeric source/sink term). When $J^u = Re_\tau^2/Re^2$ is recast in wall units, DE can be directly related to polymer-induced changes of J^u through its primary contributions (i.e. J_R^u and J_p^u) in the core region (see below for details).

Clearly, introducing polymer additive leads to a reduction in J_R^u (see figure 5*a*). This reduction becomes more pronounced as Wi is increased from 0 to 20. As Wi is further increased from 20 to 40, J_R^u is significantly enhanced, particularly in the core region. Once the viscoelastic RPCF becomes fully laminar at $Wi = 40$, the maximum in J_R^u which occurs in the core region becomes greater than the Newtonian momentum flux J^u. Meanwhile, in the range of $Wi = 20 \sim 40$, J_p^u continuously increases near the walls while slightly decreasing in the core region (see figure 5*b*). Evidently, the monotonic increase of polymer-induced DE as a function of Wi for $Wi < 20$ is facilitated by the monotonic and significant increase of J_p^u which is a source term in the momentum flux; at $Wi > 20$ J_R^u markedly increases, leading to efficient transverse momentum transport via convection.

In contrast to polymer-induced DR in wall-bounded flows that are devoid of transverse roll cells (Li *et al.* 2006; Kim *et al.* 2007; White & Mungal 2008; Pereira *et al.* 2017*a*,*b*; Teng *et al.* 2018), in viscoelastic RPCF, two maxima appear in J_p^u near the walls; these peak values increase continuously as Wi is enhanced. In fact, at high Wi these peak values approach the magnitude of the Newtonian momentum flux J^u (see figure 5*b*). The changes in J_p^u are a direct consequence of the extensional flows created at boundaries of counter-rotating transverse roll cells as depicted in figure 4. Coupled with the polymer stretching driven by the mean flow shear, these extensional flows result in enhanced polymer stress production as Wi is increased (Groisman & Steinberg 1998; Kumar & Graham 2001; Liu & Khomami 2013*a*). Consequently, the increase in the polymer stress

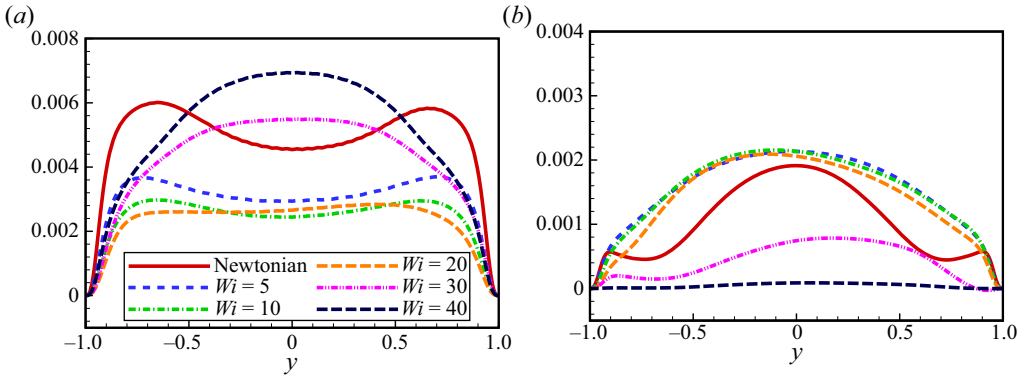

FIGURE 6. Reynolds stress decomposed into contributions of (*a*) roll cells ($J_r^u = -\langle u^r v^r \rangle$) and (*b*) turbulent vortices ($J_t^u = -\langle u'' v'' \rangle$), as $-\langle u' v' \rangle = -\langle u^r v^r \rangle - \langle u'' v'' \rangle$. Here, the variable of the roll cells is defined as $\phi^r = \langle \phi \rangle_{x,t} - \langle \phi \rangle$, and that of the turbulent vortices as $\phi'' = \phi - \langle \phi \rangle_{x,t}$, with $\langle \rangle_{x,t}$ denoting averaging in the x-direction and in time (Bech & Andersson 1996; Gai *et al.* 2016; Xia *et al.* 2019).

in the near-wall region gives rise to a monotonic increase in DE in the viscoelastic RPCF. Evidently, the magnitude of polymer stress production in this region exceeds the polymer-induced Reynolds stress reduction close to the walls (see figure 5*b*); hence, significant DE is realized.

The specific role of roll cells on polymer-induced DE can be ascertained by close inspection of figure 6. A decomposition of J_R^u into J_r^u and J_t^u, i.e. the convective momentum fluxes due to roll cells and turbulent vortices (Bech & Andersson 1996), respectively, demonstrates that J_r^u has an elastic response akin to that of J_R^u, i.e. a great decrease in the core region at $Wi < 20$ followed by a significant increase at $Wi > 20$ (see figure 6*a*). This underscores the fact that the roll cells have a dominant role in convective momentum exchange across the gap. Correspondingly, the related transverse momentum transport is weakened for $Wi < 20$ while enhanced for $Wi > 20$.

The turbulent momentum flux J_t^u shows intriguing variation versus Wi (see figure 6*b*). As Wi is enhanced, turbulent vortices exhibit a strikingly different response when compared to roll cells. Specifically, the near-wall Newtonian peaks of J_t^u become invisible upon introduction of polymer additives. This behaviour of J_t^u corresponds to the great suppression of near-wall QSV in viscoelastic RPCF (see figure 2). Interestingly, J_t^u has a small polymer-induced enhancement in the core region at $Wi = 5$ and exhibits a dome-shaped profile indicative of a very small decrease at $Wi = 5 \sim 20$. This trend underscores the fact that the momentum exchange of turbulent vortices is only slightly affected in the core region at $Wi \leq 20$. Interestingly, J_t^u becomes almost equal to J_r^u in the core region at $Wi = 20$, highlighting the fact that turbulent vortices and roll cells make equivalent contributions to the momentum exchange. In contrast, at $Wi > 20$, J_t^u becomes very small as the flow transitions to a laminar state. This observation further supports the lack of turbulent vortices in the laminar viscoelastic RPCF at $Wi = 40$ (see figure 7).

The flow physics behind the elastic response of J_t^u is further scrutinized by the polymer-induced changes of turbulent vortices depicted in figure 7. At $Wi < 20$, elongated turbulent vortices are visible and active in the core region. As Wi is increased above 20, these vortices slowly decay and finally disappear at $Wi = 40$, giving way to a laminar viscoelastic RPCF. This further rationalizes the behaviours of J_t^u in the core region, namely, momentum exchange facilitated by elongated turbulent vortices (see figure 6*b*).

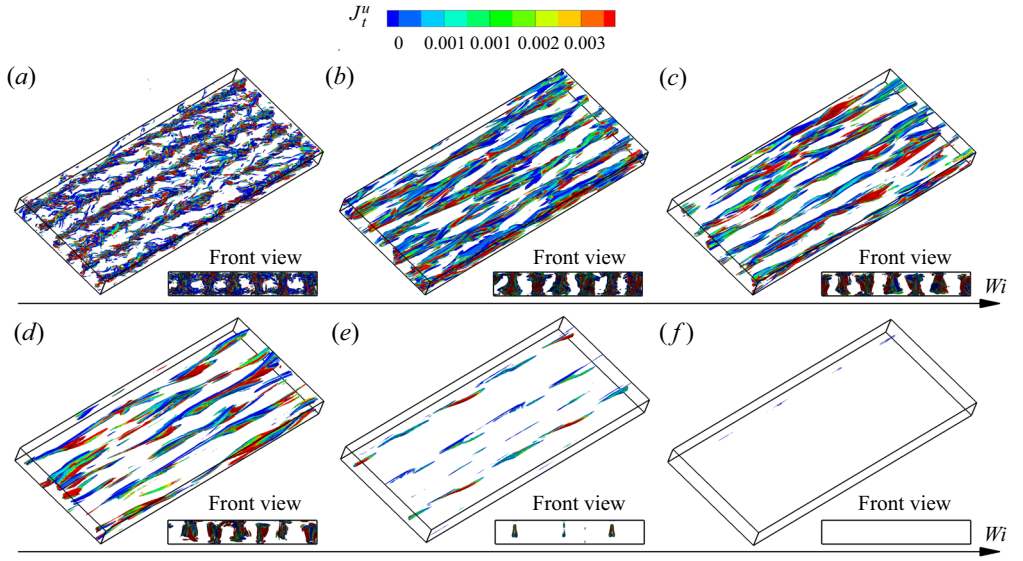

FIGURE 7. Turbulent vortices identified by Q'' and coloured by the J_t^u value. Here, Q'' is calculated by the Q-criterion based on the instantaneous fluctuating velocity (u'', v'', w''). The upper and lower plots are the full and front (x-direction) views, respectively. (a) Newtonian, $Q'' = \pm 0.5$; (b) $Wi = 5$, $Q'' = \pm 0.1$; (c) $Wi = 10$, $Q'' = \pm 0.1$; (d) $Wi = 20$, $Q'' = \pm 0.1$; (e) $Wi = 30$, $Q'' = \pm 0.1$; (f) $Wi = 40$, $Q'' = \pm 0.1$.

Furthermore, these polymer-induced changes of turbulent vortices are quite similar to that of polymer-induced transition toward MDR (Li *et al.* 2006, 2015; Kim *et al.* 2007; White & Mungal 2008; Xi & Graham 2010) via the relaminarization route (Choueiri *et al.* 2018; Lopez *et al.* 2019; Shekar *et al.* 2019; Chandra *et al.* 2020). This underscores the existence of a universal coupling dynamics between polymer chains and turbulent vortices in wall-bounded viscoelastic flows, irrespective of DR or DE. Clearly, the vortical changes illustrated in figures 2 and 7 and associated drag modifications succinctly answer the first question posed in the introduction.

The universal mechanism of the polymer–turbulence interaction can be quantified via the energy exchange terms $P_m^t / -P_p^t$ that represent energy exchange between turbulent motions and mean flow/polymer chains (Dallas, Vassilicos & Hewitt 2010; Tsukahara *et al.* 2011; Thais, Gatski & Mompean 2013; Teng *et al.* 2018). Specifically, two important features observed in the polymer-induced DR flows are demonstrated by P_m^t and $-P_p^t$ (see figure 8). First, P_m^t is positive across the gap, this corresponds to energy extraction from the main flow to the turbulent motions. Its peak value decreases gradually as Wi increases, indicating an enhanced suppression of the energy extracting process of turbulent motions. Second, the vertical flow domain is divided into three typical regions, i.e. two elastic energy storing ($-P_p^t < 0$) regions that are located in the sublayer ($y^+ \lesssim 7$) and in the core ($y^+ \gtrsim 40$) and connected by an elastic energy releasing ($-P_p^t > 0$) region in the buffer layer ($7 \lesssim y^+ \lesssim 40$). This is in accordance with the consensus established in the polymer-induced DR flows that the elastic energy stored into the stretched polymers in the sublayer and in the core is released to the turbulent motions in the buffer layer (Dallas *et al.* 2010; Xi & Graham 2010; Tsukahara *et al.* 2011; Thais *et al.* 2013; Teng *et al.* 2018). The above findings provide a substantial evidence that a universal coupling dynamics exists between polymer chains and turbulent vortices irrespective of DR or DE.

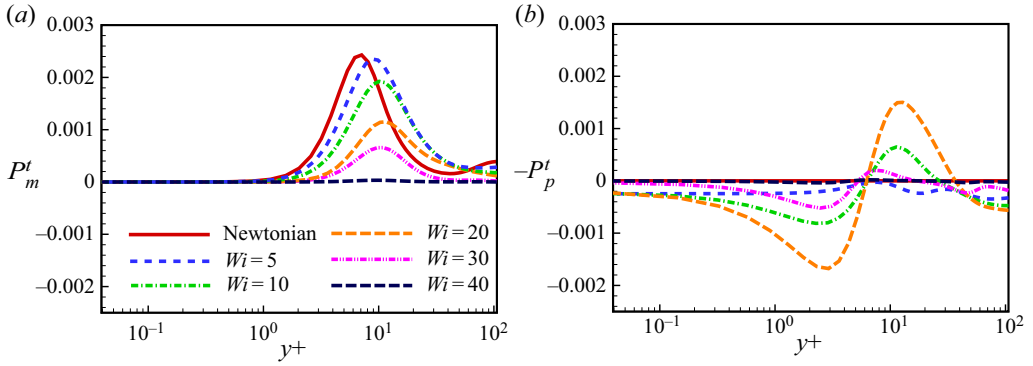

FIGURE 8. Energy exchange between turbulent motions and mean flow (a) quantified as $P^t_m = -\langle u''v''\rangle(\mathrm{d}\langle u\rangle/\mathrm{d}y)$, and that between turbulent motions and polymer chains (b) quantified as $-P^t_p = -\langle \tau'_{ik}(\partial u''_i/\partial x_k)\rangle$.

4. Concluding remarks

In summary, polymer-induced flow relaminarization has been reported for the first time for turbulent RPCF. Specifically, a reverse transition from the Newtonian turbulent RPCF to a fully relaminarized viscoelastic flow of DE occurs. The transition occurs gradually leading to elimination of small-scale vortices as Wi is enhanced, paving the way for a 2-D laminar flow consisting of large-scale and highly organized roll cells. The underlying mechanism of polymer-induced DE is elucidated in terms of transverse momentum transport, namely, the polymer stress source term (J^u_p) and the convective momentum exchange due to roll cells (J^u_r). Specifically, in the core region the increase in DE at $Wi < 20$ is ascribed to J^u_p that increases at $Wi = 5 \sim 20$, and at $Wi > 20$ to J^u_r. In the near-wall region, J^u_p increases continuously and compensates the polymer-induced near-wall reduction of convective momentum exchange. Finally, a universal mechanism of coupling dynamics between polymer chains and turbulent vortices in DR or DE inertio-elastic flows is proposed and substantiated. In addition, we are aware of the limitations of the simulation with finite Sc; nevertheless, we feel that the results obtained from the present simulations will be helpful in a physical understanding of the mechanisms of polymer-induced relaminarization.

Acknowledgements

We are grateful to Dr H. Teng and Dr Z. Xia for many helpful discussions and valuable suggestions. This work was supported by the NSFC grant 91752110, 11621202, 11572312, Science Challenge Project (no. TZ2016001) and NSF grant CBET0755269.

Declaration of interests

The authors report no conflict of interest.

Appendix

The influence of Sc and mesh size used on the reported results has been performed. To this end, test calculations were run for the RPCF of $Wi = 40$ which is of key importance as

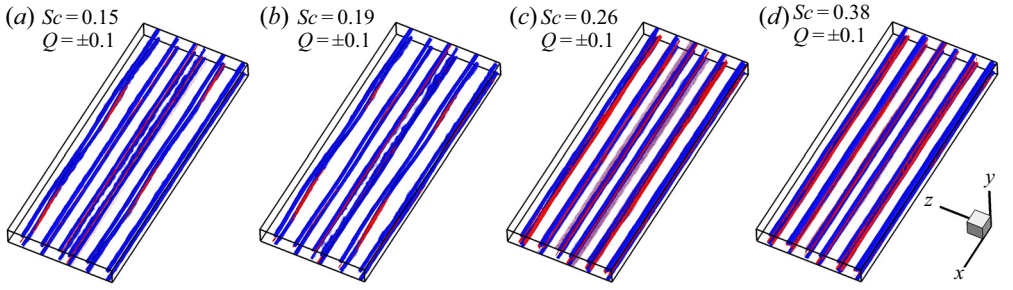

FIGURE 9. Comparison of (*a–d*) instantaneous vortical structures identified by Q-criterion at different Sc and mesh sizes. The test calculations are performed with mesh size $256 \times 129 \times 256$ (in the $x \times y \times z$ directions) for $Sc = 0.15$ and 0.19, and $512 \times 129 \times 512$ for $Sc = 0.26$ and $Sc = 0.38$.

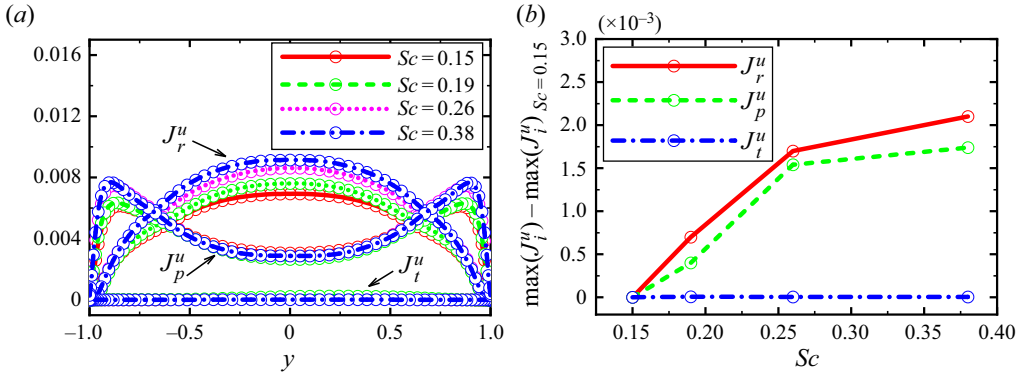

FIGURE 10. (*a*) The momentum flux associated with the polymer stress (J_p^u) and the Reynolds stress of roll cells (J_r^u) and that of turbulent vortices (J_t^u) at different Sc. (*b*) The deviation of the maximum value of J_i^u for different Sc from that for $Sc = 0.15$, where $i = r, p, t$ for J_r^u, J_p^u, J_t^u, respectively.

flow relaminarization is realized at this Wi. In our test calculations, the value of Sc is varied from 0.19 and 0.38 for mesh sizes of $256 \times 129 \times 256$ and $512 \times 129 \times 512$, respectively.

Overall, flow relaminarization has been realized at $Wi = 40$ for various Sc and different mesh sizes (see figure 9*a–d*). This laminarized RPCF with highly organized 2-D roll cells corresponds to a flow sub-regime labelled 'laminar Couette flow with straight 2-D roll cells', i.e. COU2Dh/COU2D (Tsukahara *et al.* 2010). Moreover, the momentum flux associated with the polymer stress and Reynolds stress of roll cells and that of turbulent vortices, i.e. J_p^u, J_r^u and J_t^u (see figure 10*a*,*b*), show no qualitative modifications with respect to variation in Sc. Note that J_t^u becomes practically converged, while J_p^u and J_r^u demonstrate somewhat quantitative differences when Sc is increased to 0.38 from 0.26. Nevertheless, figure 10(*b*) indicates that the quantitative influence of Sc would vanish for larger-Sc calculations performed on larger mesh sizes. This finding is consistent with the previous findings (Sureshkumar & Beris 1995; Sureshkumar *et al.* 1997) that the solution convergence is expected when Sc increases linearly with the mesh size. Hence, the present calculations can reliably reveal the underlying flow physics of the polymer-induced relaminarization.

Based on the recent work of Gupta & Vincenzi (2019) and Lopez *et al.* (2019), the high-*Re* results discussed in the present study will not be significantly affected by a further increase in *Sc*. Specifically, Gupta & Vincenzi (2019) claimed that for *Sc* values that are not excessively small quantitative rather than qualitative changes in the numerical solutions of the high-*Re* or laminar flows are expected. Furthermore, Lopez *et al.* (2019) have shown that polymer-induced relaminarization in their simulations of pipe flows using $Sc = 0.5$ is realized and have verified that this relaminarization phenomenon is a robust feature with an onset *Wi* threshold that is not altered by changing *Sc*. These previous findings taken together with our test calculations assure that the present calculations produce the essential flow features of viscoelastic RPCF.

REFERENCES

Andereck, C. D., Liu, S. S. & Swinney, H. L. 1986 Flow regimes in a circular Couette system with independently rotating cylinders. *J. Fluid Mech.* **164**, 155–183.

Bech, K. H. & Andersson, H. I. 1996 Secondary flow in weakly rotating turbulent plane Couette flow. *J. Fluid Mech.* **317**, 195–214.

Bech, K. H. & Andersson, H. I. 1997 Turbulent plane Couette flow subject to strong system rotation. *J. Fluid Mech.* **347**, 289–314.

Brauckmann, H. J., Salewski, M. & Eckhardt, B. 2016 Momentum transport in Taylor–Couette flow with vanishing curvature. *J. Fluid Mech.* **790**, 419–452.

Chandra, B., Shankar, V. & Das, D. 2020 Early transition, relaminarization and drag reduction in the flow of polymer solutions through microtubes. *J. Fluid Mech.* **885**, A47.

Choueiri, G. H., Lopez, J. M. & Hof, B. 2018 Exceeding the asymptotic limit of polymer drag reduction. *Phys. Rev. Lett.* **120** (12), 124501.

Dallas, V., Vassilicos, J. C. & Hewitt, G. F. 2010 Strong polymer-turbulence interactions in viscoelastic turbulent channel flow. *Phys. Rev.* E **82** (6), 066303.

Dubief, Y., Terrapon, V. E. & Soria, J. 2013 On the mechanism of elasto-inertial turbulence. *Phys. Fluids* **25** (11), 110817.

Dubief, Y., White, C. M., Terrapon, V. E., Shaqfeh, E. S., Moin, P. & Lele, S. K. 2004 On the coherent drag-reducing and turbulence-enhancing behaviour of polymers in wall flows. *J. Fluid Mech.* **514**, 271–280.

Dubrulle, B., Dauchot, O., Daviaud, F., Longaretti, P. Y., Richard, D. & Zahn, J. P. 2005 Stability and turbulent transport in Taylor–Couette flow from analysis of experimental data. *Phys. Fluids* **17** (9), 095103.

Gai, J., Xia, Z., Cai, Q. & Chen, S. 2016 Turbulent statistics and flow structures in spanwise-rotating turbulent plane Couette flows. *Phys. Rev. Fluids* **1** (5), 054401.

Groisman, A. & Steinberg, V. 1998 Mechanism of elastic instability in Couette flow of polymer solutions: experiment. *Phys. Fluids* **10** (10), 2451–2463.

Grossmann, S., Lohse, D. & Sun, C. 2016 High-Reynolds number Taylor–Couette turbulence. *Annu. Rev. Fluid Mech.* **48**, 53–80.

Gupta, A. & Vincenzi, D. 2019 Effect of polymer-stress diffusion in the numerical simulation of elastic turbulence. *J. Fluid Mech.* **870**, 405–418.

Kim, K., Li, C.-F., Sureshkumar, R., Balachandar, S. & Adrian, R. J. 2007 Effects of polymer stresses on eddy structures in drag-reduced turbulent channel flow. *J. Fluid Mech.* **584**, 281–299.

Kumar, K. A. & Graham, M. D. 2001 Finite-amplitude solitary states in viscoelastic shear flow: computation and mechanism. *J. Fluid Mech.* **443**, 301–328.

Li, C.-F., Sureshkumar, R. & Khomami, B. 2006 Influence of rheological parameters on polymer induced turbulent drag reduction. *J. Non-Newtonian Fluid Mech.* **140** (1–3), 23–40.

Li, C.-F., Sureshkumar, R. & Khomami, B. 2015 Simple framework for understanding the universality of the maximum drag reduction asymptote in turbulent flow of polymer solutions. *Phys. Rev.* E **92**, 043014.

LIU, N. & KHOMAMI, B. 2013*a* Elastically induced turbulence in Taylor–Couette flow: direct numerical simulation and mechanistic insight. *J. Fluid Mech.* **737**, R4.

LIU, N. & KHOMAMI, B. 2013*b* Polymer-induced drag enhancement in turbulent Taylor–Couette flows: direct numerical simulations and mechanistic insight. *Phys. Rev. Lett.* **111**, 114501.

LOPEZ, J. M., CHOUEIRI, G. H. & HOF, B. 2019 Dynamics of viscoelastic pipe flow at low Reynolds numbers in the maximum drag reduction limit. *J. Fluid Mech.* **874**, 699–719.

MARTÍNEZ-ARIAS, B., PEIXINHO, J., CRUMEYROLLE, O. & MUTABAZI, I. 2014 Effect of the number of vortices on the torque scaling in Taylor–Couette flow. *J. Fluid Mech.* **748**, 756–767.

PEREIRA, A. S., MOMPEAN, G., THAIS, L. & SOARES, E. J. 2017*a* Transient aspects of drag reducing plane Couette flows. *J. Non-Newtonian Fluid Mech.* **241**, 60–69.

PEREIRA, A. S., MOMPEAN, G., THAIS, L., SOARES, E. J. & THOMPSON, R. L. 2017*b* Active and hibernating turbulence in drag-reducing plane Couette flows. *Phys. Rev. Fluids* **2** (8), 084605.

PEREIRA, A., THOMPSON, R. L. & MOMPEAN, G. 2019 Beyond the maximum drag reduction asymptote: the pseudo-laminar state. arXiv:1911.00439.

SALEWSKI, M. & ECKHARDT, B. 2015 Turbulent states in plane Couette flow with rotation. *Phys. Fluids* **27** (4), 045109.

SAMANTA, D., DUBIEF, Y., HOLZNER, M., SCHÄFER, C., MOROZOV, A. N., WAGNER, C. & HOF, B. 2013 Elasto-inertial turbulence. *Proc. Natl Acad. Sci. USA* **110** (26), 10557–10562.

SHEKAR, A., MCMULLEN, R. M., WANG, S.-N., MCKEON, B. J. & GRAHAM, M. D. 2019 Critical-layer structures and mechanisms in elastoinertial turbulence. *Phys. Rev. Lett.* **122** (12), 124503.

SID, S., TERRAPON, V. E. & DUBIEF, Y. 2018 Two-dimensional dynamics of elasto-inertial turbulence and its role in polymer drag reduction. *Phys. Rev. Fluids* **3** (1), 011301.

SONG, J., TENG, H., LIU, N., DING, H., LU, X. & KHOMAMI, B. 2019 The correspondence between drag enhancement and vortical structures in turbulent Taylor–Couette flows with polymer additives: a study of curvature dependence. *J. Fluid Mech.* **881**, 602–616.

SURESHKUMAR, R. & BERIS, A. N. 1995 Effect of artificial stress diffusivity on the stability of numerical calculations and the flow dynamics of time-dependent viscoelastic flows. *J. Non-Newtonian Fluid Mech.* **60** (1), 53–80.

SURESHKUMAR, R., BERIS, A. N. & HANDLER, R. A. 1997 Direct numerical simulation of the turbulent channel flow of a polymer solution. *Phys. Fluids* **9** (3), 743–755.

TENG, H., LIU, N., LU, X. & KHOMAMI, B. 2018 Turbulent drag reduction in plane Couette flow with polymer additives: a direct numerical simulation study. *J. Fluid Mech.* **846**, 482–507.

THAIS, L., GATSKI, T. B. & MOMPEAN, G. 2013 Analysis of polymer drag reduction mechanisms from energy budgets. *J. Fluid Mech.* **43**, 52–61.

TSUKAHARA, T., ISHIGAMI, T., YU, B. & KAWAGUCHI, Y. 2011 DNS study on viscoelastic effect in drag-reduced turbulent channel flow. *J. Turbul.* **12**, 1468–5248.

TSUKAHARA, T., TILLMARK, N. & ALFREDSSON, P. H. 2010 Flow regimes in a plane Couette flow with system rotation. *J. Fluid Mech.* **648**, 5–33.

WHITE, C. M. & MUNGAL, M. G. 2008 Mechanics and prediction of turbulent drag reduction with polymer additives. *Annu. Rev. Fluid Mech.* **40**, 235–256.

XI, L. & GRAHAM, M. D. 2010 Turbulent drag reduction and multistage transitions in viscoelastic minimal flow units. *J. Fluid Mech.* **647**, 421–452.

XIA, Z., SHI, Y., WAN, M., SUN, C., CAI, Q. & CHEN, S. 2019 Role of the large-scale structures in spanwise rotating plane Couette flow with multiple states. *Phys. Rev. Fluids* **4** (10), 104606.